

Advanced Multi-Probe Near-Field Scanner System Utilizing Bi-polar and Phased Array Antenna Technology

E. Oblitas^{1,2}, STUDENT MEMBER, AMTA, L. Felipe Moncada-Calmet^{1,2}, STUDENT MEMBER, AMTA

Jorge L. Salazar-Cerreno^{1,2,3}, SENIOR MEMBER, AMTA

¹Advanced Radar Research Center (ARRC)

²The University of Oklahoma, Norman, OK, U.S.

³eMWave-Tech, Norman, OK, U.S.

Abstract—This paper proposes a novel approach based on a Multi-Probe Near-Field Scanner system utilizing bipolar and phased array antenna technology to measure antenna arrays with highly reliable precision. The innovative system incorporates a phased array antenna with full amplitude and phase control, enabling complete manipulation of the polarization state. This advanced capability allows the system to accurately measure and characterize antenna arrays while addressing and correcting polarization distortions caused by polar motion. By using the multi-probe configuration, the system significantly enhances measurement efficiency by capturing near-field data simultaneously across multiple probes. The integration of bipolar technology [1] ensures robust signal processing, while the phased array design enables the electronic rotation of the polarization of the probe array antenna. This feature is critical for mitigating errors introduced by polarization mismatches or distortions, ensuring high-fidelity measurements even in complex scenarios. The proposed system demonstrates superiority over traditional single-probe scanners by reducing measurement time, providing comprehensive polarization control and size reduction of the controlled environment. The paper discusses the system's design, implementation, and performance.

Index Terms—array antennas, antenna measurement, bipolar, multi-probe, near-field scan, planar near-field, polar. polarization rotation.

I. INTRODUCTION

Near-field (NF) measurements are typically categorized into three scanning geometries, spherical, cylindrical and planar. Among the planar techniques, the most common configurations are plane-rectilinear, plane-polar and plane-bipolar, being the most popular the plane-rectilinear, due to its mathematical simplicity in the NF to FF transformation process [2], [3], and the scalability without incurring into aliasing [4]; however, this configuration requires a complex mechanical system and a large controlled environment [5].

To address those limitations, different planar techniques have been developed, including the plane-polar scanning configuration, developed in the 1980's [6], [7]. These systems require a smaller controlled environment since the linear movements outwards the antenna under test (AUT) get restricted to a single dimension. In this configuration, a linear positioner takes measurements radially while AUT rotates in its own central axis, and the probe rotates to match the

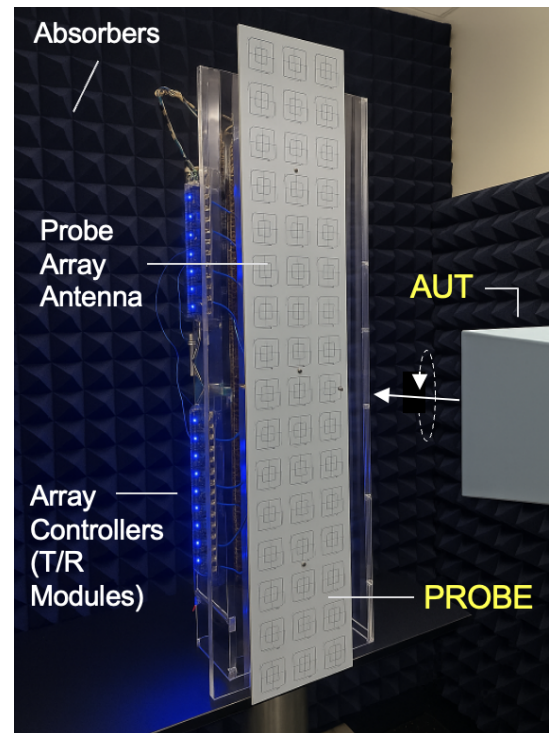


Fig. 1. Picture of the hardware side of the proposed system, showing the AUT, probe antenna array, the TR modules and the probe array controller.

polarization of the AUT, in case the probe is single polarized, for the case of dual polarized probes, it can be mathematically corrected [7], [8]. Another alternative for a planar-rectilinear configuration is the plane-bipolar technique [1], which can be carried out by replacing the linear motion of the probe by an arc motion, executed by the rotation of an arm in which end is connected the probe [9]. This combined movement causes the data to have a spiral-like shape. Although the complexity increases, faster scans could be achieved.

Additional techniques have been introduced to speed up near-field measurements, one of those is the multi-probe technique, most of whose development dates back to the

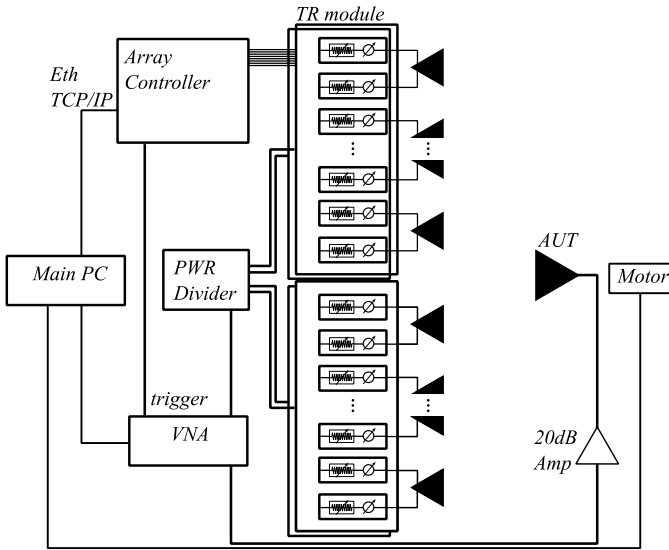


Fig. 2. Block diagram of the proposed multi-probe system

first decade of the 21st century [10], [11]. The idea is to replace the motion of a single probe by switching on and off several strategically placed probes. In this manner, the system becomes faster and less prone to mechanical issues.

In this work, both developments, i.e. multi-probe scanning and polar and bipolar scanning, are combined to create a fast and reliable near-field system that allows us to perform measurements in less time and in smaller controlled environments.

II. SYSTEM DESCRIPTION AND REQUIREMENTS

This work proposes the use of a multi-probe system to perform the plane-polar NF scanning and a similar type of bipolar NF scanning, together with the multi-probe technology allowing us to reduce the mechanical complexity of the system and reduce the test duration in comparison to the single probe systems. The idea is to use a multi-probe array with transmit/received (TR) digital modules. Each module has eight channels, which can control the magnitude through a 6-bit attenuator and phase through a 6-bit digital phase shifter.

To perform polar scanning with the probe array, it is necessary to rotate either the probe array system or the AUT. In this case, it would be more convenient to rotate the AUT since it has to be smaller than the probe array antenna, making the system mechanically simpler since it would require only one axis of motion.

However, this setup requires special corrections. Since the AUT rotates while the probe array remains stationary, the AUT's polarization also rotates relative to the probe array. Traditionally, this would require each probe antenna to rotate to maintain polarization alignment, necessitating a motor for each element and significantly increasing mechanical complexity. To avoid this, each probe antenna must be dual-polarized, enabling polarization rotation electronically by adjusting the magnitude and phase at each port. In summary, each element

in the multi-probe array must have two ports for dual polarization, with each port connected to a TR module channel for precise polarization control.

A. System Functionality

With the chosen configuration, the system requires only one motion actuator. Depending on the AUT's characteristics, this motor can be placed on either the AUT or probe side. It is typically mounted on the AUT side, as the probe array is generally larger; however, the decision also depends on the AUT's weight. The hardware is relatively simple: the system consists mainly of the probe antenna array, the antennas connected to the TR modules, and each TR module channel connected to a port of the dual-polarized probe antennas. Additionally, a probe controller embedded system configures the TR module channels, sends trigger signals to the VNA, and communicates with the main computer via TCP/IP.

As a proof of concept, the system was built using 3 GHz dual-polarized patch antennas. For multi-probe systems, it is ideal that all elements share similar electromagnetic properties—amplitude, phase, and radiation patterns. However, due to the variety of components, exact uniformity is not feasible. A calibration process, detailed in Section II-D, is used to closely match these properties. The system includes 15 active elements and 36 dummy elements (terminated ports), which help reduce refraction and edge effects, promoting uniformity. The active elements are controlled by four TR modules, each with 8 channels equipped with 6-bit digital attenuators and 6-bit digital phase shifters. The attenuator and phase shifter resolutions are 0.5 dB and 5.625° , respectively. A Copper Mountain vector network analyzer (VNA) with two RF ports is used for measurements. One port connects to the AUT through a 20 dB amplifier to compensate for system losses, while the other connects to the probe array's power divider. The RF signal path from the VNA to an antenna element involves five stages of power division, resulting in a 15 dB loss, in addition to losses from cables, attenuators, and phase shifters—making the amplifier essential. The mechanical system uses a VELMEX stepper motor for actuation. Figure 2 shows the RF system block diagram, and Fig. 1 displays most of the hardware used in the multi-probe system, excluding the main computer and VNA.

B. Multi-probe Array Design and Trade-offs

As previously explained, to perform the polar near-field scanning, either the AUT or the probe array must be rotated. To avoid the polarization mismatch produced by the rotation, a rotating linear polarization is carried out. In the literature, we can find three types of electromagnetic polarizations: linear, circular, and elliptical polarization. To begin with the explanation, we should consider the next two equations. (1) and (2) [12].

$$\mathcal{E}_x(z, t) = E_{x0} \cos(\omega t + kz + \phi_x) \hat{x} \quad (1)$$

$$\mathcal{E}_y(z, t) = E_{y0} \cos(\omega t + kz + \phi_y) \hat{y} \quad (2)$$

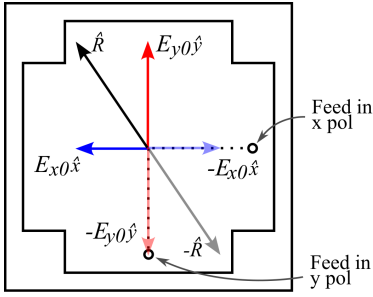


Fig. 3. Generic dual-polarized patch antenna, displaying the polarization vector (\hat{R}), conformed by the x and y polarization vectors.

Where $\mathcal{E}(z, t)$ is the electromagnetic vector in its respective axis, E_0 is the magnitude component of the vector, ω is the frequency, k is the wavenumber and ϕ is the initial phase. For this work, only linear polarization is needed; even though circular polarization also rotates the polarization, it rotates at a speed proportional to the frequency, which is way too fast even in low frequencies. The condition for obtaining linear polarization is the following.

$$\Delta\phi = |\phi_x - \phi_y| = n\pi, \quad n = 0, 1, 2, \dots \quad (3)$$

This condition only determines that the polarization is linear; however, to rotate the polarization, the terms E_{x0} and E_{y0} must be adjusted so that the resulting vector defines the desired polarization orientation. Equation (3) explains that, in order to achieve linear polarization the phase difference must be either 0 or 180, between the orthogonal ports. In (1) and (2), the magnitude components of the vector are considered positive by default. Equation (6) represents a general form for negative form of the polarization vector, where E is the magnitude of the signal and \hat{r} is the direction of the vector, as in (1) and (2). The phase must be shifted 180 to keep the linearity of the polarization. Additionally, the relation between E_{x0} and E_{y0} , as described in (5), should ideally be one. Figure 3 shows a generic dual polarized antenna with the polarization vector which is the sum of the two polarization sources. The purpose of the negative polarization vector is to rotate the resultant vector \hat{R} through all the quadrants in the plane. In addition, the equation used to calculate the rotation angle θ of the polarization vector is shown in (7).

$$\hat{R} = E_{x0}\hat{x} + E_{y0}\hat{y} \quad (4)$$

$$|\hat{R}| = \sqrt{E_{x0}^2 + E_{y0}^2} \quad (5)$$

$$-E\hat{r} = E\angle 180^\circ \hat{r} \quad (6)$$

$$\theta = \tan^{-1} \left(\frac{E_{y0}}{E_{x0}} \right) \quad (7)$$

C. Attenuator Characteristics

Equation (7) shows that θ depends mostly on the magnitude of the signals emitted in x and y polarization, while the sign

depends on the phase (ϕ_x, ϕ_y). In theory, it is possible to rotate the polarization to any angle, if the variable magnitude controller device allows it. However, the real digital attenuators or power amplifiers are components that do not have infinitesimal resolution. Since we have 6-bit digital attenuators, and our attenuation range goes from 0 to 32 dB, we can achieve a resolution of 0.5 dB per step ($\Delta\alpha$). Figure 4 displays an interesting behavior of the 6-bit attenuator. If the level of power is normalized to 1, and the attenuation transformed from dB to magnitude, then all the orange dots represent the possible polarizations; nonetheless, since we want to maintain uniformity in our measurements, the ideal attenuations will be given by the blue circles. We can observe that the errors between the ideal values and the possible ones are small enough to proceed with this methodology.

D. Probe Array Calibration

An essential process for the correct performance of the system is the characterization and calibration of the probe antennas. Due to the non-ideal characteristics of real components, it is usual that the magnitude and phase values of the emitted signal are different between ports. This irregularity will cause an error in the magnitude ($|\hat{R}|$) and rotation angle θ of the resulting polarization vector in the element. Additionally, if the elements have very different polarization vectors, errors will make the scanning result very unreliable. To compensate for the errors, a calibration process was developed. Before calibration, the required attenuation values must be determined to ensure a uniform antenna rotation angle. Our attenuator allows a minimum resolution of 1.6° , though other resolutions can be used. For instance, with a 2.5° resolution, angles from 0° to 90° are calculated using (8), and the corresponding attenuator values are obtained from (9) using x -axis projections.

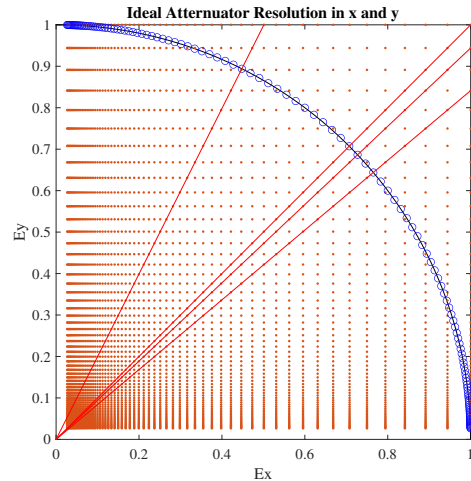


Fig. 4. 6-bit ideal attenuator values transformed from dB to magnitude for both E_{x0} and E_{y0} . Following the 6-bit characteristic of the attenuator where the red lines demonstrate that many configuration states result in the same angle, and the blue circles demonstrate all the possible angles in the ideal attenuator. The quarter circle represents the unity magnitude.

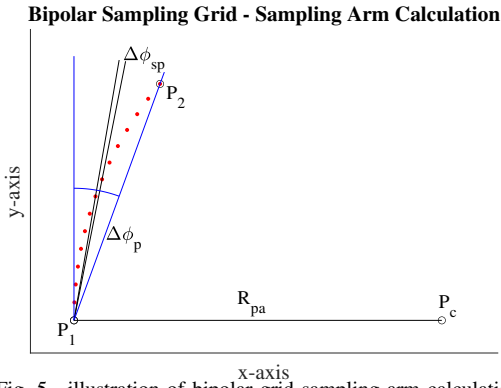


Fig. 5. illustration of bipolar grid sampling arm calculation

Values for the orthogonal polarization are derived from y -axis projections, using sine instead of cosine. In (10), α_s represents values quantized to the nearest $\Delta\alpha = 0.5$ dB. Attenuation levels can be approximated and later corrected mathematically to account for losses

$$\theta_s = 0 : \Delta\theta : \pi/2 \quad (8)$$

$$\alpha_{dB} = 20 * \log_{10}(\cos(\theta_s)) \quad (9)$$

$$\alpha_s = \text{unique}(\text{round}(\alpha_{dB}/\Delta\alpha) * \Delta\alpha) \quad (10)$$

The calibration process is straightforward; it starts by placing a mono-polarized antenna in front of each element and measuring each element in both x and y polarization, to measure the second polarization the single antenna is rotated 90 degrees. From the measured results, the lowest magnitude value is selected as the reference, so all other elements are normalized to that value. After this process, the antenna is placed back to the first antenna and the calibration algorithm starts by searching the closest attenuation and phase values that make the measured data closer to the reference. After finding the closest value to the reference, it is also necessary to calculate the closest values for the allowed attenuation values α_s needed for the polarization rotation. Due to the characteristics of the attenuator, Fig. 4, it is possible to calibrate the other state values making them relative to the reference value.

E. Operation Modes

With this design, the system can operate in two modes: a plane polar scan and a plane bipolar scan. The polar scan method is straightforward—the AUT rotates by an angle determined by the calculated sampling position and performs a rapid measurement sweep through all elements. This process repeats until all near-field (NF) spatial data around the AUT are collected.

The bipolar mode is somewhat more complex. Unlike the polar mode, where the rotor stops before each sweep, in bipolar mode the rotor moves continuously at a constant speed. The probe array takes measurements at fixed time intervals. By sampling at consistent timing while moving from the center of the AUT outward, the resulting coordinate grid forms a bipolar-type pattern.

This approach differs from the conventional bipolar system, which typically uses a double rotation mechanism. Nevertheless, the resulting spiral-shaped sampling grid has equivalent properties. Specifically, it is possible to calculate an equivalent probe arm radius using the central coordinate (P_1), the outermost point (P_2), and the tangent angle at P_1 , which is 90° as shown in Fig. 5.

$$\Delta\phi_{sp} = \frac{\Delta\phi_p}{ne - 2} \quad (11)$$

$$P_n = (x_n, y_n), \quad n = 1, 2, c \quad (12)$$

$$m = -\cot(90^\circ) \quad (13)$$

$$x_c = \frac{x_1^2 - x_2^2 - (y_1 - y_2)^2}{2(x_1 - x_2 + m(y_1 - y_2))} \quad (14)$$

$$y_c = m(x_c - x_1) + y_1 \quad (15)$$

Where $\Delta\phi_p$ is the angular sampling resolution [4], ne is the number of elements, $\Delta\phi_{sp}$ is the angular sampling spacing between elements of the probe array. Equation (14) show the formula to calculate the center coordinate and radius of the imaginary probe arm. This information is necessary in the calculation of the near-field to far-field transformation for the bipolar measurement not involving interpolation [4].

With the multi-probe design it is possible the perform the measurements by placing the AUT in the center element of the probe array and only rotate 180° to make a complete measurement, limiting the range of the scanning to the half of the length of the probe array. Or, with AUT placed a the corner element perform the data collection by completely rotating the AUT a whole round and extending the range by two compared to the former setup.

III. MEASUREMENT RESULTS

To test the performance of the multi-probe bi-polar measurement system, a 3 GHz 15 dB gain horn antenna was used as AUT, The AUT was placed in an external corner of the probe array for a large array.

A. Measurements

Both polar and bipolar scannings where performed, the smallest circle enclosing the AUT in the $x-y$ plane is 25 cm, resulting in a sampling angle resolution of 10° . The duration of the polar scanning was 100.82 seconds. While in the bipolar scan had also a sampling angle of 10° . With 15 elements minus the center one, the 10° is divided by 14 resulting in 0.714° , which is the angle spacing between probe array element sampling. The duration of the scanning was 96.02 seconds. Figure 6 illustrates the polar NF results of the raster, polar and bipolar scanning, both magnitude and phase.

B. Results Comparison

To measure the performance of the scanning system, a comparison with a reference NF measurement is needed, in this case, the reference is the NF measurement of a common raster scanning. Due to mechanical limitation of the positioners, the scanning range is 0.4 m in the x -axis and 0.7 m in the y -axis.

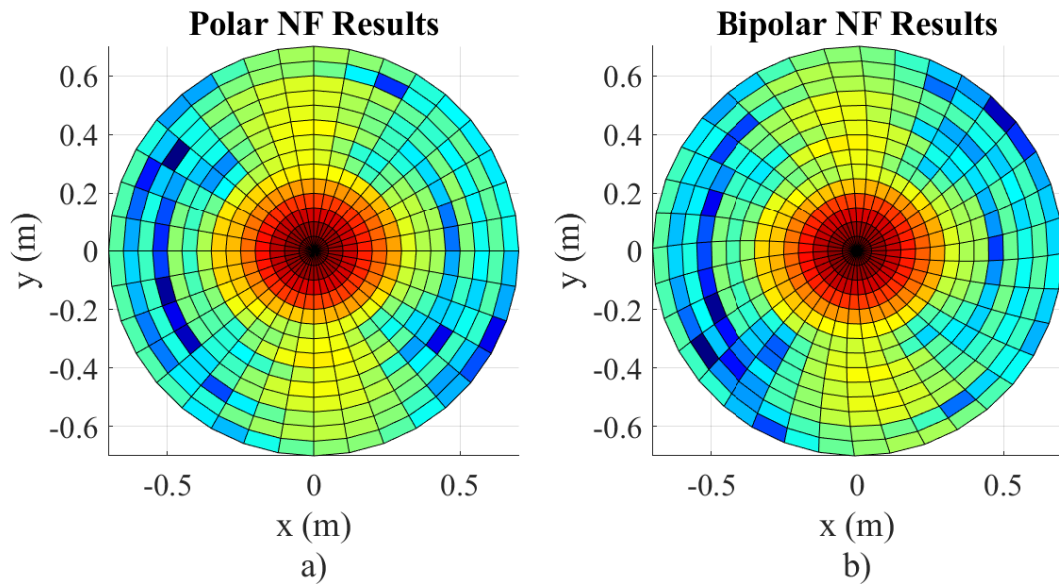


Fig. 6. a) Near-field results of a 3 GHz 15 dB gain horn antenna using the plane polar NF scanning. b) NF results of the same antenna using the plane bipolar method,

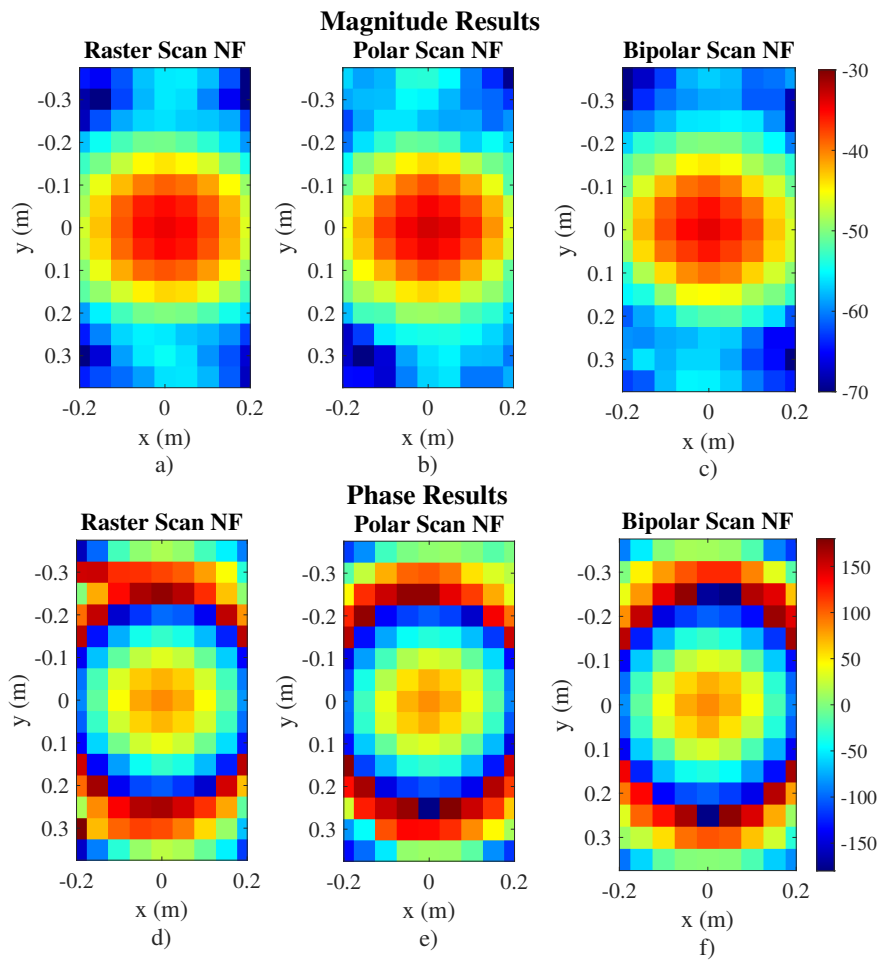


Fig. 7. Near-field results comparison, a) and d) are the results of the raster scan (reference) magnitude and phase respectively. b) and e) are the results of the polar scan magnitude and phase respectively. c) and f) results of the bipolar scan.

In previous sections, it is mention that a way to perform a near-field to far-field transformation of the polar and bipolar results is by interpolation into a cartesian coordinates. Figure 7.a and .b illustrates the NF results of a raster scan, while the rest show the interpolated data of the polar and bipolar. The interpolation of the two datasets was performed to enable their comparison with the reference and to use the exact same algorithm of near-field to far-field transformation and compare the radiation patterns. Figure 8 and 9 illustrates the radiation pattern of both E-plane and H=-plane respectively. The reason why in E-plane show a larger θ_{ff} angle in the plot is due to the size of the scanning range where the y -axis is larger than the x -axis. From the plots, it is evident that the radiation patterns across the various systems are highly similar, which signifies that the NF results are likewise closely matched.

IV. CONCLUSIONS

The implemented proof of concept system was designed for S-band. However, this can be scaled to other frequencies, although new hardware such as the probe antenna array and TR modules would need to be redesign. Furthermore, in this prototype, patch antennas were used as probe antennas due to its size being equal to half wavelength, but they are not the best option to NF systems due to the narrow frequency bandwidth. Future research could focus on the development of a dual-polarized probe antenna with a physical size of less than half wavelength.

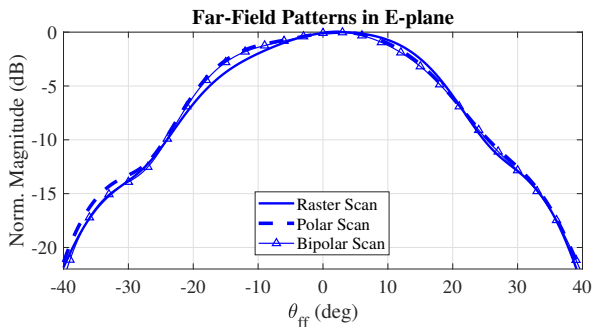


Fig. 8. Far-field radiation pattern's E-plane of the 3 GHz horn antenna

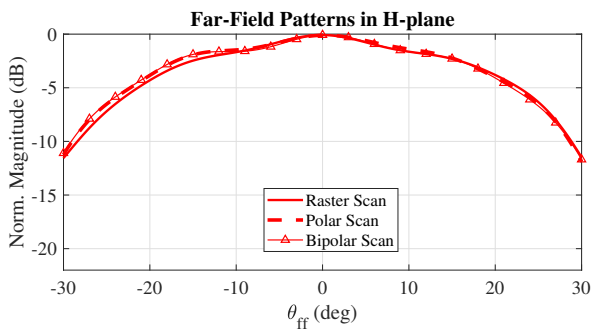


Fig. 9. Far-field radiation pattern's H-plane of the 3 GHz horn antenna

TR modules used in the prototype system were originally design for phase array antenna systems, those devices were not design for fast switching, making them a little inefficient in the speed aspect. That is the reason why the bipolar mode is just slightly faster than the polar mode. However, the design can be improved to enable faster switching, thereby reducing the scanning duration of the bipolar mode.

As previously illustrated, the reliability of the results is high, making it a successful measurement system that can be improved. Furthermore, the greatest advantage this system provides is the large range of measurement in the smallest possible volume of the system. The size of the system can be even reduced by increasing the frequency, where most of the components size are reduced.

ACKNOWLEDGEMENT

This work is supported by Advance Radar Research Center (ARRC), The University of Oklahoma and eMWave-tech. Any opinions, findings, conclusions, or recommendations expressed in this material are those of the author(s) and do not necessarily reflect the views of ARRC, The University of Oklahoma and eMWave-tech

REFERENCES

- [1] Y. Rahmat-Samii, L. Williams, and R. Yaccarino, "The ucla bi-polar planar-near-field antenna-measurement and diagnostics range," *IEEE Antennas and Propagation Magazine*, vol. 37, no. 6, pp. 16–35, 1995.
- [2] *Near-Field Scanning Measurements: Theory and Practice*, 2008, pp. 929–976.
- [3] S. Gregson, J. McCormick, and C. Parini, "Principles of planar near-field antenna measurements," *Bibliovault OAI Repository, the University of Chicago Press*, vol. 53, 01 2008.
- [4] S. Costanzo and G. D. Massa, "Advanced numerical techniques for near-field antenna measurements," in *Numerical Simulations of Physical and Engineering Processes*, J. Awrejcewicz, Ed. Rijeka: IntechOpen, 2011, ch. 15. [Online]. Available: <https://doi.org/10.5772/23203>
- [5] T. Brockett and Y. Rahmat-Samii, "A novel portable bipolar near-field measurement system for millimeter-wave antennas: construction, development, and verification," *IEEE Antennas and Propagation Magazine*, vol. 50, no. 5, pp. 121–130, 2008.
- [6] Y. Rahmat-Samii and M. Gatti, "Far-field patterns of spaceborne antennas from plane-polar near-field measurements," *IEEE Transactions on Antennas and Propagation*, vol. 33, no. 6, pp. 638–648, 1985.
- [7] Y. Rahmat-Samii, V. Galindo-Israel, and R. Mittra, "A plane-polar approach for far-field construction from near-field measurements," *IEEE Transactions on Antennas and Propagation*, vol. 28, no. 2, pp. 216–230, 1980.
- [8] F. Larsen and J. Hansen, "A dual-polarized probe system for near-field measurements," in *1979 Antennas and Propagation Society International Symposium*, vol. 17, 1979, pp. 557–560.
- [9] L. Williams and Y. Rahmat-Samii, "Novel bi-polar planar near-field measurement scanner at ucla," in *Antennas and Propagation Society Symposium 1991 Digest*, 1991, pp. 1446–1449 vol.3.
- [10] P. Iversen, P. Garreau, and D. Burrell, "Real-time spherical near-field handset antenna measurements," *IEEE Antennas and Propagation Magazine*, vol. 43, no. 3, pp. 90–94, 2001.
- [11] L. J. Foged, L. Duchesne, A. Rosa, D. Belot, and J. M. Lopez, "High gain p-band antenna measurements in multi probe spherical near field range," in *2010 14th International Symposium on Antenna Technology and Applied Electromagnetics the American Electromagnetics Conference*, 2010, pp. 1–4.
- [12] C. A. Balanis, *Antenna Theory: Analysis and Design*. USA: Wiley-Interscience, 2016.